Journal of Power Sources 203 (2012) 115–120

Contents lists available at SciVerse ScienceDirect

Journal of Power Sources

journal homepage: www.elsevier.com/locate/jpowsour

Short communication

Synthesis of $Li[Li_{1.19}Ni_{0.16}Co_{0.08}Mn_{0.57}]O_2$ cathode materials with a high volumetric capacity for Li-ion batteries

Hyo-Jin Kim [a], Hun-Gi Jung [a,b], Bruno Scrosati [a,c,*], Yang-Kook Sun [a,b,*]

[a] Department of Energy Engineering, Hanyang University, Seoul 133-791, South Korea
[b] Department of Chemical Engineering, Hanyang University, Seoul 133-791, South Korea
[c] Department of Chemistry, University of Rome Sapienza, 00185, Rome, Italy

ARTICLE INFO

Article history:
Received 7 October 2011
Received in revised form
27 November 2011
Accepted 28 November 2011
Available online 7 December 2011

Keywords:
Lithium-ion batteries
Cathode materials
Coprecipitation synthesis
Tap density
Volumetric capacity

ABSTRACT

Microscale $Li[Li_{0.19}Ni_{0.16}Co_{0.08}Mn_{0.57}]O_2$ powders with a high tap density were synthesized using $[Ni_{0.2}Co_{0.1}Mn_{0.7}]O_x$ precursor with a unique microstructure via coprecipitation in flowing air. The synthesized $Li[Li_{0.19}Ni_{0.16}Co_{0.08}Mn_{0.57}]O_2$ powders were composed of spherical nanosized primary particles, which results in a high tap density due to the high packing of the spherical primary particles. When used as electrode in a lithium cell, $Li[Li_{0.19}Ni_{0.16}Co_{0.08}Mn_{0.57}]O_2$ exhibits a very high gravimetric capacity of 263 mAh g^{-1} and a volumetric capacity of 956 mAh cm^{-3}, as well as an excellent rate capability delivering a discharge capacity of 202 mAh g^{-1} at a 2 C-rate. TEM analysis together with SEM observations show that the electrochemical performance of the $Li[Li_{0.19}Ni_{0.16}Co_{0.08}Mn_{0.57}]O_2$ electrode is primarily governed by its microstructure.

1. Introduction

The exhaustion of natural resources along with environmental concerns of greenhouse gas emissions has led to significant development of lithium-ion batteries for plug-in hybrid vehicle (PHEV) and electric vehicle (EV) applications. However, commercialization of these batteries in automobiles requires further increases of their energy density and cycle life as well as cost reductions. The most promising cathode materials for automotive applications are Ni-rich $Li[Ni_{1-x}M_x]O_2$ ($x \leq 0.2$) compounds, which can deliver a capacity of 200 mAh g^{-1} and are relatively cheap [1,2]. However, a couple of candidate materials, $Li[Ni_{0.8}Co_{0.15}Al_{0.05}]O_2$ and $Li[Ni_{0.8}Co_{0.1}Mn_{0.1}]O_2$, have shown poor thermal stabilities due to the release of oxygen, which oxidizes the organic electrolyte and thus, leads to severe thermal runaway, thus increasing the safety hazard of the cell [3–5]. Some studies have been conducted to develop new high-capacity cathode materials meeting the energy requirements for PHEV and EV applications [6,7]. Currently, a composite material containing spinel Li–Mn–O and layered Li–Ni–Mn–O is being used for the practical automobile applications because the composite exhibits a relatively stable thermal stability even though its resulting capacity is smaller than that of $Li[Ni_{1-x}M_x]O_2$ [8–10].

Recently, Li-rich layered oxides with composite structures $(xLi_2MnO_3 \cdot (1-x)LiMO_2$, M = Ni, Co, Mn, etc.. . .) have been extensively studied as promising cathode materials in high energy batteries for transportation applications [11–14]. These materials deliver a very high discharge capacity of 240–280 mAh g^{-1} between 2.0 and 4.8 V. However, there are still several major issues to be resolved including their (i) poor rate capability, (ii) large irreversible capacity at the 1st cycle, (iii) significant discharge voltage decrease upon cycling, and (iv) low powder tap density. Although the poor rate capability and the 1st cycle irreversible capacity have been improved by surface modification of the cathode with AlF_3, $AlPO_4$, and Al_2O_3 coating [15–17], there have been only a few studies aiming to obtain an increase in the powder tap density [18–20]. As well known, the tap density of an active material has a key practical importance since it reflects in the value of its volumetric capacity.

In this paper, we report a microscale oxide-$Li[Li_{0.19}Ni_{0.16}Co_{0.08}Mn_{0.57}]O_2$ electrode material prepared by an optimized synthesis procedure via co-precipitation in flowing air using a $[Ni_{0.2}Co_{0.1}Mn_{0.7}]O_x$ precursor. We show that this electrode has a very high tap density and excellent electrochemical properties when cycled in a lithium cell.

2. Experimental

Hydroxide $[Ni_{0.2}Co_{0.1}Mn_{0.7}](OH)_2$ and oxide $[Ni_{0.2}Co_{0.1}Mn_{0.7}]O_x$ precursors were synthesized by a coprecipitation method.

* Corresponding authors at: Department of Energy Engineering, Hanyang University, Seoul 133-791, South Korea. Tel.: +82 2 2220 0524; fax: +82 2 2282 7329.
E-mail addresses: Bruno.Scrosati@uniroma1.it (B. Scrosati), yksun@hanyang.ac.kr (Y.-K. Sun).

0378-7753/$ – see front matter © 2011 Elsevier B.V. All rights reserved.
doi:10.1016/j.jpowsour.2011.11.076

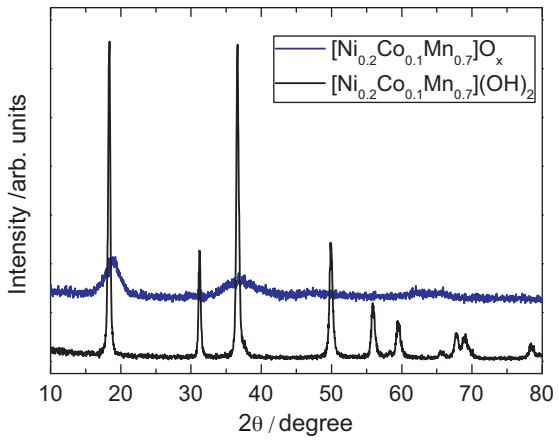

Fig. 1. X-ray diffraction patterns of the $[Ni_{0.2}Co_{0.1}Mn_{0.7}](OH)_2$ and $[Ni_{0.2}Co_{0.1}Mn_{0.7}]O_x$ powders.

An aqueous solution containing $NiSO_4{\cdot}6H_2O$, $CoSO_4{\cdot}7H_2O$, and $MnSO_4{\cdot}5H_2O$ at a concentration of 2.0 mol dm^{-3} was pumped into a continuously stirring tank reactor (CSTR) with a capacity of 4 L. At the same time, a 2.0 mol dm^{-3} NaOH solution and a desired amount of a NH_4OH solution were also seperately fed into the reactor. Inside the reactor, an atmosphere of flowing nitrogen and air was used for the synthesis of the hydroxide $[Ni_{0.2}Co_{0.1}Mn_{0.7}](OH)_2$ and oxide $[Ni_{0.2}Co_{0.1}Mn_{0.7}]O_x$, respectively. The detailed synthetic procedures are described in our previous papers [21,22]. The mixture of precursor hydroxide (or oxide) with $LiOH{\cdot}H_2O$ was preheated at 500 °C for 5 h and calcined at 900 °C for 10 h in air to obtain crystalline $Li[Li_{0.19}Ni_{0.16}Co_{0.08}Mn_{0.57}]O_2$.

The chemical compositions of the resulting powders were analyzed by atomic absorption spectroscopy (AAS, Vario 6, Analyticjena). The crystalline phases of the synthesized products were characterized by powder X-ray diffraction (XRD, Rint-2000, Rigaku) measurements using Cu Kα radiation. The particle morphologies of the powders were evaluated using scanning electron microscopy (SEM, JSM 6400, JEOL) and transmission electron microscopy (TEM, JEOL, 2010). The surface areas of the powders were measured by

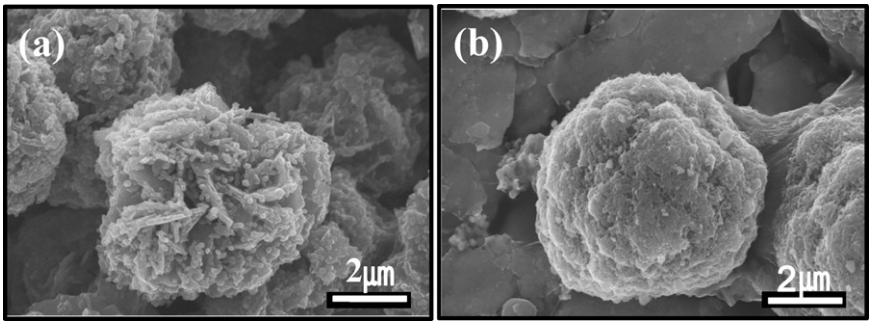

Fig. 2. SEM images of the (a) $[Ni_{0.2}Co_{0.1}Mn_{0.7}](OH)_2$ and (b) $[Ni_{0.2}Co_{0.1}Mn_{0.7}]O_x$ powders.

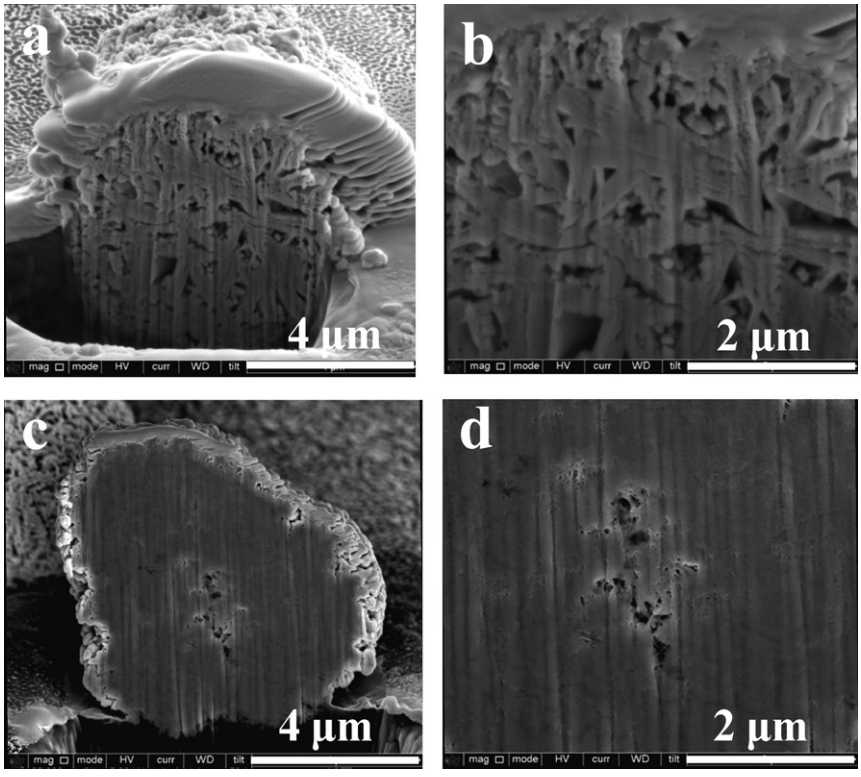

Fig. 3. Cross-sectional SEM images of $[Ni_{0.2}Co_{0.1}Mn_{0.7}](OH)_2$ at (a) low and (b) high magnifications, and $[Ni_{0.2}Co_{0.1}Mn_{0.7}]O_x$ at (c) low and (d) at high magnifications.

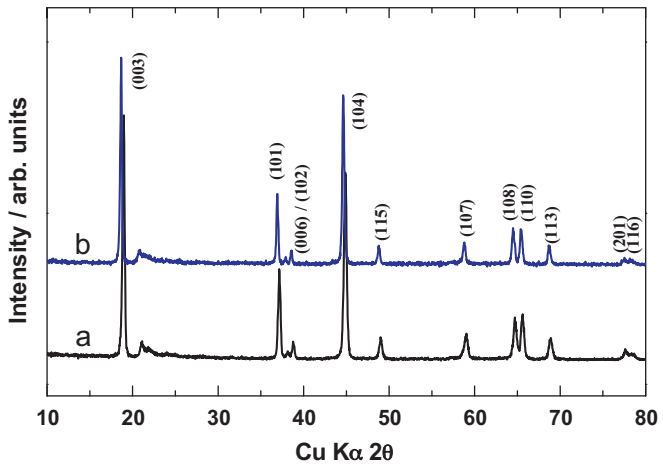

Fig. 4. X-ray diffraction patterns of the (a) hydroxide-Li[$Li_{0.19}Ni_{0.16}Co_{0.08}Mn_{0.57}$]$O_2$ and (b) oxide-Li[$Li_{0.19}Ni_{0.16}Co_{0.08}Mn_{0.57}$]$O_2$ powders.

nitrogen adsorption using the Brunauer–Emmett–Teller method (AS1-A4, Quantachrome).

The electrochemical performances of the synthesized cathodes were assessed using a 2032 coin-type cell. The cell consisted of a cathode and a lithium metal anode separated by a porous polypropylene film. The electrodes consisted of a mixture of the prepared powder, carbon black, and polyvinylidene fluoride (85:7.5:7.5 wt.%) in N-methyl-2-pyrrolidone. The slurry was spread onto aluminum foil and dried in a vacuum oven at 110 °C. The loading of the electrodes was in average of 6 mg cm^{-2}. The electrolyte used was 1 M $LiPF_6$ in a 3:7 mixture, by volume, of ethylene carbonate (EC) and dimethyl carbonate (DMC) (PANAX ETEC Co., Ltd, Korea).

3. Results and discussion

The quality of any cathode material strongly depends on its synthesis procedure. Hydroxide coprecipitation is a very well known and effective method used to synthesize lithium transition metal oxides with high purity [21]. Recently, we reported the synthesis of spherical xLi_2MnO_3–$yLi[Ni_{1/3}Co_{1/3}Mn_{1/3}]O_2$–$zLiNiO_2$ powders ($0.48 \le x \le 0.60$, $0.32 \le y \le 0.40$, and $0.0 \le z \le 0.2$) powders by a hydroxide coprecipitation method [19]. The powders produced by the hydroxide process possess good homogeneity with a well defined chemical composition and spherical morphology. However, it is difficult to synthesize Li-rich (or Mn-rich) layered materials with a high tap density by hydroxide coprecipitation because $Mn(OH)_2$ has an inherently plate-shaped morphology, which is resistant to tighter packing of the primary particles, and is readily oxidized or decomposed during the coprecipitation reaction. Recently, we successfully synthesized spherical $Li_{1.05}M_{0.05}Mn_{1.9}O_4$ (M = Ni, Mg, Al) spinel oxides using a spherical $(M–Mn)_3O_4$ precursor via co-precipitation [22].

In this work, we have further optimized the synthesis procedure to obtain micro-sized (5 μm), secondary Li[$Li_{0.19}Ni_{0.16}Co_{0.08}Mn_{0.57}$]$O_2$ particles (hereafter referred to as oxide) composed of nano-sized primary particles (100 nm) using [$Ni_{0.2}Co_{0.1}Mn_{0.7}$]O_x precursor via coprecipitation in flowing air. For comparison, we also synthesized the same Li[$Li_{0.19}Ni_{0.16}Co_{0.08}Mn_{0.57}$]$O_2$ material (hereafter referred to as hydroxide), using $Ni_{0.2}Co_{0.1}Mn_{0.7}(OH)_2$ and a conventional hydroxide process.

The average chemical compositions of the two as-prepared materials were nearly identical, determined by AAS to be Li[$Li_{0.19}Ni_{0.16}Co_{0.08}Mn_{0.57}$]$O_2$ by AAS. Fig. 1 shows the X-ray diffraction patterns of the [$Ni_{0.2}Co_{0.1}Mn_{0.7}$]$(OH)_2$ and [$Ni_{0.2}Co_{0.1}Mn_{0.7}$]O_x precursors. The prepared [$Ni_{0.2}Co_{0.1}Mn_{0.7}$]$(OH)_2$ has the typical crystalline structure of layered $M(OH)_2$ [23]. On the contrary, [$Ni_{0.2}Co_{0.1}Mn_{0.7}$]O_x has a low mixed oxide and hydroxide crystalline structure. The SEM images of Fig. 2a and b shows that the [$Ni_{0.2}Co_{0.1}Mn_{0.7}$]$(OH)_2$ and [$Ni_{0.2}Co_{0.1}Mn_{0.7}$]O_x materials have both a spherical morphology with average particle diameters around 5–6 μm. However, the [$Ni_{0.2}Co_{0.1}Mn_{0.7}$]$(OH)_2$ precursor particles are composed of long rectangular primary particles due to the inherent plate-type shape of $Mn(OH)_2$, which pills loosely to form a slightly, quasi-spherical structure. On the contrary, the [$Ni_{0.2}Co_{0.1}Mn_{0.7}$]O_x particles consist of nano-sized spherical primary particles. It is noted that the [$Ni_{0.2}Co_{0.1}Mn_{0.7}$]$(OH)_x$ precursor has a powder tap density of 1.2 g cc^{-1} while that of the [$Ni_{0.2}Co_{0.1}Mn_{0.7}$]O_x precursor is considerably higher, i.e., 1.5 g cc^{-1}.

Fig. 3 shows the cross-sectional images of the [$Ni_{0.2}Co_{0.1}Mn_{0.7}$]$(OH)_2$ and [$Ni_{0.2}Co_{0.1}Mn_{0.7}$]O_x particles prepared by a focused ion beam cut. Clearly, numerous pores are revealed by the magnified SEM image of the [$Ni_{0.2}Co_{0.1}Mn_{0.7}$]$(OH)_2$ particles, showing that the pores are formed within the loosely agglomerated long rectangular primary particles (Fig. 3b); hence, the low powder tap density of the [$Ni_{0.2}Co_{0.1}Mn_{0.7}$]$(OH)_2$ precursor. On the contrary, the [$Ni_{0.2}Co_{0.1}Mn_{0.7}$]O_x secondary particles are closely piled with fine spherical primary particles resulting in a much less porous structure and finally in a higher tap density (Fig. 3d). Indeed, the tap density of these electrode materials has been measured to be 1.92 g cc^{-1} and their BET surface area 1.73 m^2 g^{-1}.

Fig. 4 shows the XRD patterns with the Miller indices of the two Li[$Li_{0.19}Ni_{0.16}Co_{0.08}Mn_{0.57}$]$O_2$ powders. All of the diffraction

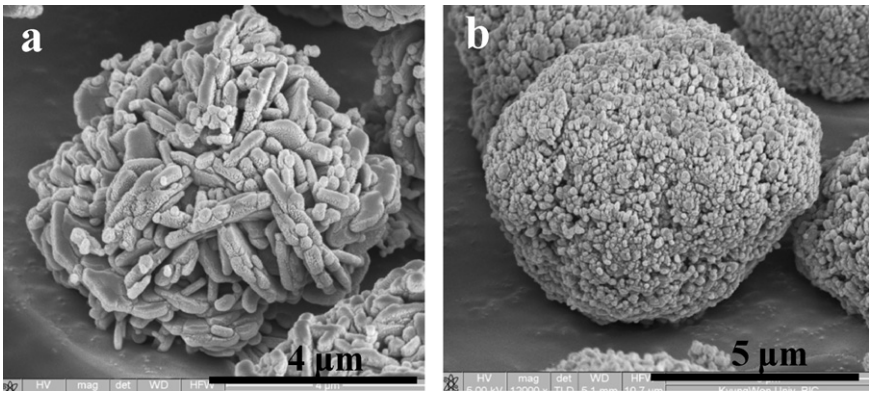

Fig. 5. SEM images of the (a) hydroxide-Li[$Li_{0.19}Ni_{0.16}Co_{0.08}Mn_{0.57}$]$OH_2$ and (b) oxide-Li[$Li_{0.19}Ni_{0.16}Co_{0.08}Mn_{0.57}$]$O_2$ powders.

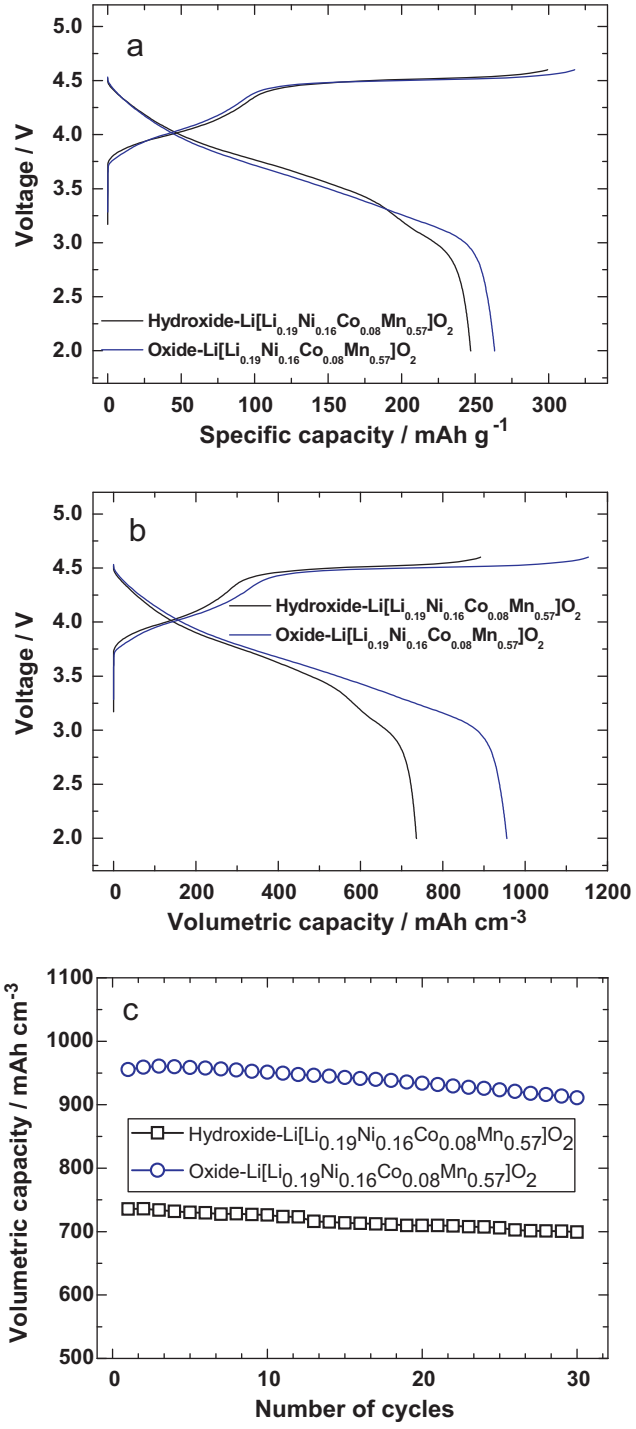

Fig. 6. Comparison of the initial charge and discharge curves of the hydroxide-$Li[Li_{0.19}Ni_{0.16}Co_{0.08}Mn_{0.57}]O_2$ and oxide-$Li[Li_{0.19}Ni_{0.16}Co_{0.08}Mn_{0.57}]O_2$ powders: (a) gravimetric capacity, (b) volumetric capacity, and (c) cycling response. Voltage range: 2.0–4.6 V. Rate: 20 mA g^{-1}. Room temperature.

peaks can be indexed based on a hexagonal α-$NaFeO_2$ structure with a space group of $R\bar{3}m$ except for the weak peaks present between 20 and 25°. These peaks are characteristic of a complex Li_2MnO_3–$LiMO_2$ phase, resulting from the ordering of metal ions (Li, Ni, and Mn) and the existence of a Li_2MnO_3 phase [24]. Another observation in the XRD patterns is the clear splitting of the (0 0 6)/(0 1 2) and (0 1 8)/(1 1 0) peaks, indicating that the material has a well organized layered structure.

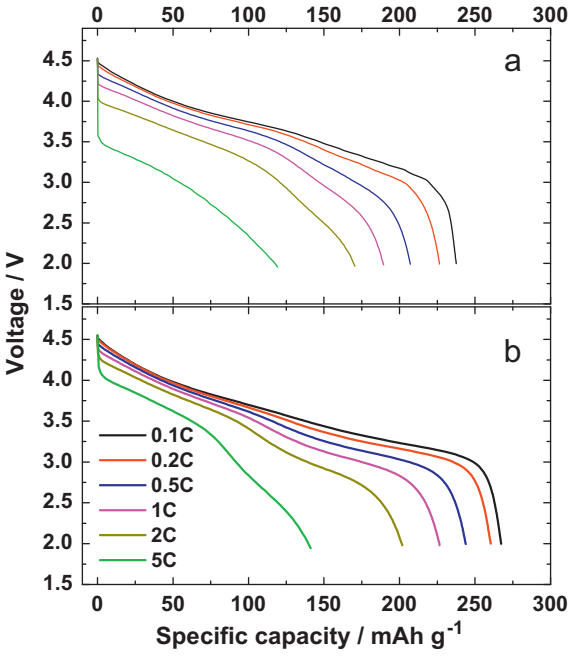

Fig. 7. Comparison of the discharge curves of the (a) hydroxide-$Li[Li_{0.19}Ni_{0.16}Co_{0.08}Mn_{0.57}]O_2$ and (b) oxide-$Li[Li_{0.19}Ni_{0.16}Co_{0.08}Mn_{0.57}]O_2$ powders as a function of the C-rate. Voltage range: 2.0–4.6 V. Room temperature.

Regardless to the negligible difference in their chemical composition and crystalline phases, there is an obvious difference in the primary particle sizes and the tap densities of the two materials. Fig. 5 shows SEM images of the two lithiated $Li[Li_{0.19}Ni_{0.16}Co_{0.08}Mn_{0.57}]O_2$ powders. As expected, the spherical and the average particle diameter of the precursors were retained after calcination at high temperature. In particular, Fig. 5a shows that the size of the primary particles of the hydroxide-$Li[Li_{0.19}Ni_{0.16}Co_{0.08}Mn_{0.57}]O_2$ is larger and that these particles are agglomerated more closely than in the case of $[Ni_{0.2}Co_{0.1}Mn_{0.7}](OH)_2$ (compare Fig. 5b); however, many voids among the primary particles within the spherical secondary particles are still present. On the contrary, the spherically-shaped oxide-$Li[Li_{0.19}Ni_{0.16}Co_{0.08}Mn_{0.57}]O_2$ particles are composed of closely piled, nano-sized primary particles with diameters of about 200 nm (Fig. 5b) and this explains why the tap density of the oxide-$Li[Li_{0.19}Ni_{0.16}Co_{0.08}Mn_{0.57}]O_2$ powders is much higher than that of the hydroxide-$Li[Li_{0.19}Ni_{0.16}Co_{0.08}Mn_{0.57}]O_2$ powders, namely 1.95 g cc^{-1} versus 1.52 g cc^{-1}. As expected, the BET surface area of the oxide-$Li[Li_{0.19}Ni_{0.16}Co_{0.08}Mn_{0.57}]O_2$ is lower than that of the hydroxide-$Li[Li_{0.19}Ni_{0.16}Co_{0.08}Mn_{0.57}]O_2$, namely 1.73 m^2 g^{-1} versus 2.35 m^2 g^{-1}.

The electrochemical performances of both hydroxide- and oxide-$Li[Li_{0.19}Ni_{0.16}Co_{0.08}Mn_{0.57}]O_2$ powders were determined by standard tests performed with a R2032 coin-type half-cell employing Li metal as the negative electrode. Fig. 6a compares the initial charge–discharge voltage profiles of the two $Li[Li_{0.19}Ni_{0.16}Co_{0.08}Mn_{0.57}]O_2$ electrodes based on their specific gravimetric capacity. Both electrodes show two distinguishable voltage regions in the course of the charge process. The first charging capacity of 110 mAh g^{-1}, observed below 4.45 V, is associated with the $Ni^{2+/4+}$ oxidation reaction, which is consistent with the theoretical capacity of 112 mAh g^{-1} based on 0.53 $Li[Ni_{0.38}Co_{0.19}Mn_{0.44}]O_2$ 0.47 Li_2MnO_3 (or $Li[Li_{0.19}Ni_{0.16}Co_{0.08}Mn_{0.57}]O_2$). The electrodes exhibit then a voltage plateau around 4.5 V, which is associated with the simultaneous removal of Li^+ and O^{2-} (as Li_2O) from the

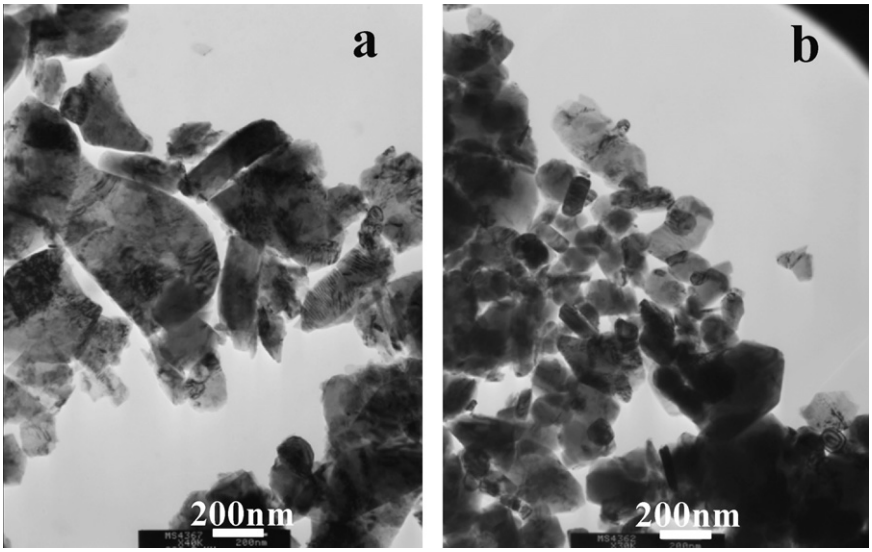

Fig. 8. High resolution TEM images of the (a) hydroxide-$Li[Li_{0.19}Ni_{0.16}Co_{0.08}Mn_{0.57}]O_2$ and (b) oxide-$Li[Li_{0.19}Ni_{0.16}Co_{0.08}Mn_{0.57}]O_2$ powders.

Li_2MnO_3 component [25–28]. The observed discharge capacities of the hydroxide and oxide-$Li[Li_{0.19}Ni_{0.16}Co_{0.08}Mn_{0.57}]O_2$ electrodes were 247 and 263 mAh g^{-1}, respectively. Based on their respective densities, the gravimetric capacities were converted into volumetric capacities and the respective voltage curves are shown in Fig. 6b. The volumetric capacity delivered by the oxide-$Li[Li_{0.19}Ni_{0.16}Co_{0.08}Mn_{0.57}]O_2$ electrode, i.e., 955.6 mAh cm^{-3} is, at the same 0.1 C-rate, 1.3 times higher than that of the hydroxide-$Li[Li_{0.19}Ni_{0.16}Co_{0.08}Mn_{0.57}]O_2$, i.e., 735.7 mAh cm^{-3}. This capacity difference is a direct consequence of the difference in the tap density of the two electrodes. Finally, although with consistent differences in the values of the capacity delivery, both electrodes showed good cycling response, with capacity retentions of 95% after 30 cycles, see Fig. 6c.

Fig. 7 compares the discharge profiles of the Li/hydroxide- and of Li/oxide-$Li[Li_{0.19}Ni_{0.16}Co_{0.08}Mn_{0.57}]O_2$ cells as a function of the C-rate between 2.0 and 4.6 V. For this test, the cells were charged galvanostatically at a 0.1 C-rate and then discharged at C-rates ranging from 0.1 to 5 C-rates (20–1000 mA g^{-1}). It can be clearly observed that the capacity delivery of the oxide-$Li[Li_{0.19}Ni_{0.16}Co_{0.08}Mn_{0.57}]O_2$ electrode is higher at all C-rates. For example, at 2 C-rate the capacity of the oxide-$Li[Li_{0.19}Ni_{0.16}Co_{0.08}Mn_{0.57}]O_2$ electrode amounts to 202 mAh g^{-1} versus the 169 mAh g^{-1} obtained by the hydroxide-$Li[Li_{0.19}Ni_{0.16}Co_{0.08}Mn_{0.57}]O_2$ electrode.

The difference in electrochemical performance is further explained by examining the microstructures of the two materials. Fig. 8 shows bright-field TEM images of the hydroxide- and oxide-$Li[Li_{0.19}Ni_{0.16}Co_{0.08}Mn_{0.57}]O_2$ particles. Fig. 8a reveals that the primary particles of the hydroxide-$Li[Li_{0.19}Ni_{0.16}Co_{0.08}Mn_{0.57}]O_2$ sample have an average size of 1 μm with a sharp rectangular shape, with associated irregular morphology resulting in poor electrochemical performances. In contrast, the oxide-$Li[Li_{0.19}Ni_{0.16}Co_{0.08}Mn_{0.57}]O_2$ consists of much finer primary spherical particles whose sizes ranges from 100 to 200 nm, see Fig. 8b. The nano-size of the primary particles reduces the lithium diffusion pathway, so greatly increasing the rate capability of the electrode. Despite the structural transition, there is no substantial difference in the microscopic particle morphology of the as-precipitated $[Ni_{0.2}Co_{0.1}Mn_{0.7}]O_x$ precursor and that of oxide-$Li[Li_{0.19}Ni_{0.16}Co_{0.08}Mn_{0.57}]O_2$, which indicates that lithium is readily incorporated into the primary structure.

4. Conclusions

In this paper we report the physical and electrochemical characteristics of a microscale $Li[Li_{0.19}Ni_{0.16}Co_{0.08}Mn_{0.57}]O_2$ electrode prepared by an optimizing synthesis procedure. We show that this electrode material, composed of spherical primary particles, has a higher packing density than parent $Li[Li_{0.19}Ni_{0.16}Co_{0.08}Mn_{0.57}]OH_2$ hydroxide materials formed by irregular primary particles. This difference is explaining by considering that spherical particles have a reduced contacting interface among the primary particles and thus, few vacancies in their packing structure. Hence, the oxide-$Li[Li_{0.19}Ni_{0.16}Co_{0.08}Mn_{0.57}]O_2$ electrode is characterized by an unusually high tap density that reflects in an enhanced rate capability and volumetric energy density when cycled in a lithium cell. For all these properties, we believe that the $Li[Li_{0.19}Ni_{0.16}Co_{0.08}Mn_{0.57}]O_2$ electrode here reported is of definite interest for the lithium battery community.

Acknowledgments

This research was supported by WCU (World Class University) program through the Korea Science and Engineering Foundation by Education, Science, and Technology (R31-10092) and the National Research Foundation of Korea (NRF) grant funded by the Korea government (MEST) (No. 2009-0092780).

References

[1] R. Kostecki, F. McLarnon, Electrochem. Solid-State Lett. 7 (2004) A380.
[2] M.-H. Kim, H.-S. Shin, D. Shin, Y.-K. Sun, J. Power Sources 159 (2006) 1328.
[3] H. Arai, S. Okada, Y. Sakurai, J. Yamaki, Solid State Ionics 109 (1998) 295.
[4] S.-W. Woo, S.-T. Myung, H. Bang, D.-W. Kim, Y.-K. Sun, Electrochim. Acta 54 (2009) 3851.
[5] H. Konishi, T. Yuasa, M. Yoshikawa, J. Power Sources 196 (2011) 6884.
[6] Y.-K. Sun, S.-T. Myung, B.-C. Park, J. Prakash, I. Belharouak, K. Amine, Nat. Mater. 8 (2009) 320.
[7] N. Recham, J.-N. Chotard, L. Dupont, C. Delacourt, W. Walker, M. Armand, J.-M. Tarascon, Nat. Mater. 9 (2010) 68.
[8] T. Numata, C. Amemiya, T. Kumeuchi, M. shirakata, M. Yonezawa, J. Power Sources 97–98 (2001) 358.
[9] H. Kitao, T. Fujihara, K. Takeda, N. Nakanishi, T. Nohma, Electrochem. Solid-State Lett. 8 (2005) A87.
[10] S.-T. Myung, K.-S.Lee, Y.-K. Sun, H. Yashiro, J. Power Sources 196 (2011) 7039.
[11] Lu, D.D. MacNeil, J.R. Dahn, Electrochem. Solid-State Lett. 4 (2001) A191.
[12] S.-S. Shin, Y.-K. Sun, K. Amine, J. Power Sources 112 (2002) 634.
[13] S.-H. Kang, Y.-K. Sun, K. Amine, Electrochem. Solid-State Lett. 6 (2003) A183.

[14] C.S. Johnson, J.-S. Kim, C. Lefier, N. Li, J.T. Vaughey, M.M. Thackeray, Electrochem. Commun. 6 (2004) 1085.
[15] Y. Wu, A. Manthiram, Electrochem. Solid-State Lett. 9 (2006) A221.
[16] J.M. Zheng, Z.R. Zhang, X.B. Wu, Z.X. Dong, Z. Zhu, Y. Yang, J. Electrochem. Soc. 155 (2008) A775.
[17] Y. Wu, A. Vadivel Murugan, A. Manthiram, J. Electrochem. Soc. 155 (2008) A635.
[18] H. Deng, I. Belharouak, Y.-K. Sun, K. Amine, J. Mater. Chem. 19 (2009) 4510.
[19] J.-H. Lim, H. Bang, K.S. Lee, K. Amine, Y.-K. Sun, J. Power Sources 189 (2009) 571.
[20] H. Deng, I. Belharouak, R.E. Cook, H. Wu, Y.-K. Sun, K. Amine, J. Electrochem. Soc. 157 (2010) A447.
[21] M.-H. Lee, Y.-J. Kang, S.-T. Myung, Y.-K. Sun, Electrochim. Acta 50 (2004) 939.
[22] K.-S. Lee, S.-T. Myung, H.J. Bang, S. Chung, Y.-K. Sun, Electrochim. Acta 52 (2007) 5201.
[23] Joint Committee on Powder Diffraction Standards, Card No. 14-0117.
[24] C.S. Johnson, N. Li, C. Lefief, M.M. Thackeray, Electrochem. Commun. 9 (2007) 787.
[25] Z. Lu, J.R. Dahn, J. Electrochem. Soc. 149 (2002) A778.
[26] J.-S. Kim, C.S. Johnson, J.T. Vaughey, M.M. Thackeray, S.A. Hackney, W. Yoon, C.P. Grey, Chem. Mater. 16 (2004) 1996.
[27] A.R. Armstrong, M. Holzhapfel, P. Novak, C.S. Johnson, S.-H. Kang, M.M. Thackeray, P.G. Bruce, J. Am. Chem. Soc. 128 (2006) 8694.
[28] C.S. Johnson, J.-S. Kim, C. Lefief, N. Li, J.T. Vaughey, M.M. Thackeray, Electrochem. Commun. 6 (2004) 1085.